HHS Public Access

Author manuscript

J Mech Behav Biomed Mater. Author manuscript; available in PMC 2019 September 01.

Published in final edited form as:

J Mech Behav Biomed Mater. 2018 September ; 85: 152–161. doi:10.1016/j.jmbbm.2018.05.044.

Bone healing response in cyclically loaded implants:

Comparing zero, one, and two loading sessions per day

Renan de Barros e Lima Bueno[a], **Ana Paula Dias**[a], **Katia J. Ponce**[a], **Rima Wazen**[a], **John B. Brunski**[b], **Antonio Nanci**[a,*]

[a]Laboratory for the Study of Calcified Tissues and Biomaterials, Faculty of Dentistry, Université de Montréal, Montreal, QC, Canada

[b]Department of Surgery, School of Medicine, Stanford University, Stanford, CA, United States

Abstract

When bone implants are loaded, they are inevitably subjected to displacement relative to bone. Such micro-motion generates stress/strain states at the interface that can cause beneficial or detrimental sequels. The objective of this study is to better understand the mechanobiology of bone healing at the tissue-implant interface during repeated loading. Machined screw shaped Ti implants were placed in rat tibiae in a hole slightly bigger than the implant diameter. Implants were held stable by a specially-designed bone plate that permits controlled loading. Three loading regimens were applied, (a) zero loading, (b) one daily loading session of 60 cycles with an axial force of 1.5 N/cycle for 7 days, and (c) two such daily sessions with the same axial force also for 7 days. Finite element analysis was used to characterize the mechanobiological conditions produced by the loading sessions. After 7 days, the implants with surrounding interfacial tissue were harvested and processed for histological, histomorphometric and DNA microarray analyses. Histomorphometric analyses revealed that the group subjected to repeated loading sessions exhibited a significant decrease in bone-implant contact and increase in bone-implant distance, as compared to unloaded implants and those subjected to only one loading session. Gene expression profiles differed during osseointegration between all groups mainly with respect to inflammatory and unidentified gene categories. The results indicate that increasing the daily cyclic loading of implants induces deleterious changes in the bone healing response, most likely due to the accumulation of tissue damage and associated inflammatory reaction at the bone-implant interface.

Keywords

Bone; Implant; Loading; Micromotion; Histomorphometry; Gene expression

*Correspondence to: Laboratory for the Study of Calcified Tissues and Biomaterials, Department of Stomatology, Faculty of Dentistry, Université de Montréal, P.O. Box. 6128, Station Centre-Ville, Montreal, QC, Canada H3C 3J7. antonio.nanci@umontreal.ca.

Declarations of interest

None.

Appendix A. Supplementary material

Supplementary data associated with this article can be found in the online version at http://dx.doi.org/10.1016/j.jmbbm.2018.05.044.

1. Introduction

Since bone implants unquestionably will remain a mainstream treatment modality for years to come, a better understanding and control of the healing events at the bone-implant interface – where cell fate decisions are made – is mandatory to meet these challenges, especially in the cases where implants are immediately loaded after placement. When implants are loaded, they are subjected to some degree of micromotion; the displacement of the implant relative to bone generates stress and strain that will result in the local deformation of supporting interfacial tissues (Brunski, 1999; Haiat et al., 2014). Micromotion and the ensuing local tissue deformation can affect bone healing, cause fibrous encapsulation, induce bone resorption, and lead to implant loosening (discussed in Wazen et al., 2013a), all of which generate morbidity and ultimately require implant replacement. However, it has been suggested that some degree of micromotion can also positively influence bone formation (Birkhold et al., 2014; Duyck et al., 2007, 2006; Geris et al., 2008; Leucht et al., 2007; Vandamme et al., 2007a, 2007b; Willie et al., 2010; Yang et al., 2013; Zhang et al., 2014).

Most loading studies have examined the healing process around implants using an experimental system in which constant micromotion of the implant is applied, which can then require an increase in loading force throughout the healing period as the interface attempts to heal (Leucht et al., 2007; Wazen et al., 2013a). Clinically, subjects typically use overall similar forces during mastication but the period during which force is exerted varies. In this context, few studies have evaluated the interfacial bone healing response with respect to the number of sessions per day of implant loading. Finally, since virtually all implants have an initial interface with at least some gaps between the cut bone and implant surface, it remains important to study the influence of loading on induction of new bone in such gaps. This latter point has motivated our study of events in a Bone Implant Gap Interface (BIGI) and follows up on our prior work in a murine tibia model where constant displacement was applied (Leucht et al., 2007; Wazen et al., 2013a).

The focus of our work is not to replicate any particular clinical situation but rather to investigate the basic bone healing response that occurs near the bone-implant interface where tissue deformation takes place during loading. A rat tibia model was used for correlation of multiple analytical approaches, including DNA microarray, histological, and biomechanical analyses. We hypothesized that the cumulative number of cycles of force (and related interfacial strain) per day can affect events in this gap interface that will fill, or not, with bone. Our data shows that despite no increase in peak applied force, simply doubling the number of loading sessions (and cumulative cycles) per day has a significant influence on healing at the bone implant interface, a point that should be taken into consideration when evaluating clinical loading regimens.

2. Materials and methods

2.1. Ti implants and surface analysis

Machined screw-shaped implants made of cp Titanium Grade 2 (Medical Micro Machining Inc, Colfax, WA, USA) were used. The surface quality of the screws was checked using a

JEOL JSM-7400F field emission scanning electron microscope (SEM) operated at 1–2 kV. The screws were 7 mm length, 0.45 mm pitch and 1.7 mm diameter. Before surgery, samples were washed with 70% ethanol and air-dried.

2.2. Type of interface and surgical procedure

The screw shaped titanium implants were placed in 2.0 mm holes in rat tibiae to create a model of gap-healing at an interface (BIGI, (Wazen et al., 2013a)). Twenty-seven male Wistar rats weighting 200–225 g (Charles Rivers Canada; St-Constant, QC, Canada) were anesthetized with an intraperitoneal injection of a mixture of Ketalean (0.05 mg/g body weight; ketamine hydrochloride; Biomeda-MTC, Cambridge, ON, Canada), Rompun (0.005 mg/g body weight; xylazine; Bayer Inc., Toronto, ON, Canada) and Acevet (0.001 mg/g body weight; acepromazine maleate; Vetoquinol Inc., Lavaltrie, QC, Canada). The anteromedial side of each hind limb was shaved and cleaned with Baxedin® (chlorhexidine gluconate; Omega Laboratories, Montreal, QC, Canada). A 1 cm incision was made through the skin using a 15 C blade (Almedic, Montreal, QC, Canada). The skin and muscle were gently pried apart to expose the periosteum. Using holes near the extremities of the bone plate as guide, two unicortical holes were drilled in bone at low speed using a 0.5 mm drill bit (Drill Bit City, Prospect Heights, IL, USA) and titanium alloy retopins (0.62 mm in diameter) were placed through the holes in the bone plate and into the cortices of the bone, thereby fixing the bone plate to the bone. With the center column of the bone plate as a guide, a main transcortical hole was drilled, at the superior level of the antero-medial tibial metadiaphysis, at low speed using a 2.00 mm diameter drill bit (Drill Bit City). Titanium implants were then inserted into the hole with a silicone rubber O-ring (Apple Rubber Products, Lancaster, NY, USA) situated between the head of the implant and the center column of the bone plate. The cap was screwed onto the center column of the bone plate (Fig. 1). The skin incision was closed around the central column of the Delrin plate using 4-0 Vicryl sutures (Ethicon, Inc, Somerville, NJ, USA) and surgical staples (Becton Dickinson, Franklin Lakes, NJ, EUA) The surgical site was again cleaned and disinfected with Baxedin® (Omega Laboratories). The animals received an injection of Temgesic® (0.2 ml Buprenorphine hydrochloride, Reckitt and Colman, Hull, UK) after surgery, and were fed with soft food containing Temgesic® (Reckitt and Colman).

2.3. Micromotion system and loading regimen

The micromotion system used was sized for use in the rat tibia, but was otherwise identical to the system that we previously used in mice (Leucht et al., 2007; Wazen et al., 2013b, Fig. 1A and C–F). A hand-held Force Gauge Series 5, model M7-2 loading device (Fig. 1B, Mark-10, Copiague, NY, USA) was used to apply controlled force to the implant through a small opening in the top of the protective cap. The loading device – − 2 lb = 8.896 N capacity – can be used in tension or compression and is factory-calibrated, with a maximum error in full scale reading of 0.03%. We checked its performance in our own calibration trials where we recorded the force gauge's output in response to application of known weights. Three loading regimens were applied for 7 days, ***(a)*** zero loading (Unloaded group) (***b***) one daily loading session of 60 cycles with an axial force of 1.5 N/cycle (Micromotion 1× group), and (***c***) two daily sessions of 60 cycles each session with the same force per cycle (Micromotion 2× group). Loading frequency was controlled manually and the approximate

rate of loading was 1 cycle per second. For the one and two daily loading sessions groups, the animals were anesthetized and kept under AErrane anesthesia (isoflurane USP, Baxter, Mississauga, ON, Canada) maintained at 1–2% during application of force. Hence, these loaded animals were anesthetized one and two times per day, respectively. The surgical site was cleaned once a day with Baxedin® (Omega Laboratories) before the loading and, the unloaded group was also similarly anesthetized once a day for routine wound cleaning. Each isoflurane anesthesia including the induction never exceeded 5 min. The experimental groups and loading protocols are described in Table 1.

2.4. Ethical approval and animal supervision

All animal procedures and experimental protocols were approved by the Comité de déontologie de l'expérimentation sur les animaux of Université de Montréal. Animals were under regular observation at the University animal facilities throughout the period of experimentation. They were given food and water ad libitum and left to move around freely in the cages. The animals' appearance, weight and healing were checked on a daily basis. All sections of this report adhere to the ARRIVE Guidelines for reporting animal research.

2.5. Finite element analysis

To clarify the biomechanical environment over time around unloaded and loaded implants, 3-D finite element (FE) models were formulated (Fig. 2A and B). The geometry of the implant site in the rat tibia was modeled as a 4 mm-diameter composite cylinder made up of a 0.6 mm layer of cortical bone with a 1.6 mm-thick layer of trabecular bone beneath it in the marrow, plus a drill hole (2 mm in diameter, 2.2 mm deep) containing the 1.7 mm-diameter implant. The drill hole was filled with fibrin or healing tissue, depending upon time after implantation. The outer boundaries of the model (except for the top of the bone cylinder) were constrained. The properties of the cortical bone, trabecular bone that forms in the marrow cavity, interfacial region, and implant were as described in Table 2. Note that in simulating the situation immediately after implantation – when the gap interface is filled with a fibrin clot – we assigned the properties of fibrin to the gap (Munster et al., 2013).

In loading the implant, we accounted for the fact that a 1.5 N axial force on the implant in the bone plate system is balanced by a force from the O-ring (beneath the head of the screw) plus a force from the interface on the screw threads, i.e., not all of the force applied to the screw head is transferred to the implant's interface. The amount of force taken by the O-ring vs. interface – and, in turn, the displacement of the implant – depends on the properties of the interface, e.g., with no tissue in the interfacial gap, our experiments showed that the implant moved 93.7 μm when 1.5 N was applied to the screw. (The axial stiffness of the O-ring was 0.016 N/micron.)

The FE model also allowed us to vary the properties of the gap tissue to estimate how healing (or lack thereof) in the gap interface would cause the interface's stiffness to change over time after implantation. We also used FE models to compute the strain state in the interface when the applied force on the implants remained the same throughout the 7 days of the experiments.

2.6. Tissue processing for histology

Animals were anesthetized with a mixture of a 20% chloral hydrate solution (0.4 mg/g body weight Sigma-Aldrich Canada Ltd, Oakville, ON, Canada) and Rompun (0.005 mg/g body weight; xylazine; Bayer Inc) and sacrificed by an inhalation overdose of AErrane (isoflurane USP, Baxter). Tibias were dissected and immersed in a fixative solution consisting of 4% paraformaldehyde and 0.1% glutaraldehyde in 0.1 M phosphate buffer, pH 7.2 overnight at 4 °C. The samples were then decalcified for 3 days at 4 °C in Planck-Rychlo solution consisting of 0.13 M aluminium chloride hexahydrate (Sigma-Aldrich), 0.2 N hydrochloric acid (Fisher Scientific, Whitby, ON, Canada), 1.35% formic acid (Fisher Scientific) and then the implants were removed carefully. Decalcified samples were washed for 24 h in 0.1 M phosphate buffer (pH 7.2), dehydrated through graded ethanols, cleared with xylene, embedded in paraffin and serially-sectioned at 5 μm thickness. Some sections were stained with hematoxylin and eosin and others with toluidine blue for observation by light microscopy and histomorphometric analyses.

2.7. Histomorphometric analyses

Five animals were used for each group (n = 5) and 12 serial sections were cut spanning the surgical site in each animal. One section was selected near the beginning, middle and end of the serial section sequence. Three sections per animal were thus analyzed for a total of 15 sections per group. The bone formation area **(BFA)**, the distance between the implant surface and the first appearance of bone (bone implant distance, **BID**), and the percentage of implant surface in contact with bone **(BIC)** were measured. For BFA two measurements were carried out in, *(1)* the area delimited by the 2 mm drill used to create the BIGI surgical hole to place the implants and the implant surface [a distance of 0.15 mm on each side] **(BFA_0)** and (2) the area delimited by the inner diameter (3.75 mm) of the trephine used to sample the tissues for molecular analyses (see below) and the implant surface [a distance of 1.025 on each side] **(BFA_t)**. In both cases, the measurements extended from the upper aspect of the cortex and also included an area extending 10 μm from the bottom of the implants. The **BID** was calculated using the mean bone–implant distance over the entire implant periphery based on data taken from 30 evenly spaced points around the periphery of the implant in each section, for a cumulative number of 90 measurements per animal. The **BIC** and **BID** measurements were carried out from the first thread down toward the third one on both sides.

The Image-J software (NIH, Bethesda, MD, USA) was used for all histomorphometric analyzes. The software transforms high definition microscopic pictures into binary images, allowing to calculate area and pixel values. For the measurements of the “bone pixels” present in the interest area, the maximum threshold was 175. Histological analyses were carried out by a different person than the one that placed the implants, on slides that were identified simply with an experimental number.

2.8. Histomorphometric statistical analyses

The Shapiro-Wilk test was used to verify the data normality using Origin Pro 8.5 software (OriginLab Corporation, Northampton, MA, USA.). Kolmogorov-Smirnov or two sample tests with 95% confidence intervals were performed to determine the differences in BFA,

BID and BIC for unloaded and loaded groups. Values of $p < 0.05$ were considered statistically different.

2.9. Tissue processing for RNA extraction

After 7 days, animals were anesthetized with a mixture of 20% chloral hydrate solution (0.4 mg/g body weight; Sigma-Aldrich) and Rompun (0.005 mg/g body weight; xylazine; Bayer Inc.), the wound was cleaned with 70% ethanol and opened with a scalpel blade and the protective cap and the implant were gently removed. The implant was immediately placed in 1 ml of Trizol (Invitrogen, Burlington, ON, Canada), vortexed for 1 min to release any surface adherent tissue into the Trizol and then removed. Under RNAlater (Fisher Scientific) irrigation, the exposed bone surface was gently cleaned to minimize contamination by soft tissues, and the bone at the surgical site (including cortical and newly formed trabecular bone around the medullary portion of the implant) was harvested using a cold 3.75 mm diameter trephine drill (#04-9482-01, ACE Dental Implant System, Brockton, MA, USA) fitted on a slow-speed hand piece (Physiodispenser 4000, Henry Schein Inc., Niagara On The Lake, ON, Canada). After the drilling, the bone was cut into smaller pieces (≤ 0.5 cm) under RNAlater and placed after in a sterilized Eppendorf™ Snap-Cap Microcentrifuge Safe-Lock™ Tubes (Fisher Scientific) containing RNAlater solution (Fisher Scientific) for 48 h. The RNAlater was completed removed, the Trizol used to extract RNA from the implant (se above), was added and the bone was homogenized with a Polytron® (Kinematic Inc., Bohemia, NY) at full speed for 1 min. Total RNA was extracted from the samples as recommended by manufacturer and purified with the RNeasy® MiniElute® Cleanup kit (Qiagen, Mississauga, ON, Canada). RNA samples were placed in tubes numbered non descriptively for subsequent blind analysis. RNA concentration, integrity and quality were analyzed using the Agilent Bioanalyzer 2100 at the McGill University and Génome Québec Innovation Centre (Montréal, QC, Canada). Only RNA samples showing well-defined 18s and 28s ribosomal RNA peaks and with a high RNA integrity number (RIN > 8.5) were considered of enough quality to be used for the microarray analyses. A sample size of $n = 4$ for each group was used.

2.10. DNA microarray design, hybridization, data normalization and analysis

The GeneChip Rat Gene 2.0 ST Array (Affymetrix, Santa Clara, CA, USA) was used for DNA microarray analysis. The chip is designed to have a minimum sensitivity of 1:100,000. This concentration ratio corresponds roughly to a few copies of transcript per cell, or an approximate 1.5 pM concentration. The assay was performed at the *Genome Québec Innovation Centre* (McGill University, Montreal, QC, Canada). Briefly, sense-strand cDNA was synthesized from 100 ng of total RNA, and fragmentation and labeling were performed to produce ss DNA with the Affymetrix GeneChip® WT Terminal Labeling Kit according to manufacturer's instructions. After fragmentation and labeling, 3.5 μg DNA target was hybridized on GeneChip® Rat Gene 2.0 ST and incubated at 45 °C in the GeneChip® Hybridization oven 640 (Affymetrix) for 17 h at 60 rpm. GeneChips were then rinsed in a GeneChips® Fluidics Station 450 using Affymetrix Hybridization Wash and Stain kit according to the manufacturer's instructions. The microarrays were finally scanned on a GeneChip® scanner 3000 (Affymetrix).

Extensive analyses of microarray data were performed using the Affymetrix® Expression Console™ software for gene level normalization and signal summarization, and then the Affymetrix Transcriptome Analysis Console (TAC) software for exploration and differential gene expression analysis. The Gene Ontology (GO) analyses for up- and down regulated genes were performed using the PANTHER Classification System (http://www.pantherdb.org/). Pathway analyses of differentially expressed genes were carried out using the Ingenuity Pathway Analysis (IPA) software (Qiagen Bioinformatics, Redwood City, CA, USA).

2.11. Gene expression statistical analyses

Comparisons were performed using a parametric test for independent data (ANOVA) by Transcriptome Analysis Console (TAC) Software. The cut off for the fold-change in gene expression was 2 and the level of significance was set at 5%

3. Results

3.1. Histology and histomorphometric analysis

After surgical implantation and loading sessions, there were no clinical signs of distress, and infection or inflammation at the wound site. In all groups, the animals gained around 50 g during the experiments.

Trabecular bone formed in the marrow cavity around the implants and active surfaces of bone deposition were observed in all cases (Fig. 3). There were no histological signs of major inflammatory infiltrate at the surgical sites. There were also no differences in the overall distribution of new bone at the surgical implantation site in all groups. There was, however, evidence of disrupted bone formation and connective tissue formation right near the implant surface in the Micro-motion 2× group (Fig. 3C) and, in a single case, some cartilage formation was observed (Fig. 4). In this single case, the cartilage was situated near the flank of a thread and at the base of the implant, which is where cartilage tissue might be expected to form given the local strain states (e.g., negative hydrostatic stress and large distortional strain). While, as expected, osteoclasts were present at the surgical site, in all cases, no conspicuous accumulation of osteoclasts were observed.

The histomorphometric analyses confirmed the histological findings; for the $\mathbf{BFA_t}$ analysis, no major difference was measured between the groups in the bone volume defined by the overall trephine diameter area ($p > 0.05$, Fig. 5A). However, in the $\mathbf{BFA_0}$ analysis, the Micro-motion 2× group showed a significantly lower percentage of bone area formation when compared with the other two groups ($p < 0.05$,Fig. 5A). The Micromotion 2× group also showed a lower percentage of **BIC** ($p < 0.05$, Fig. 5B), and an overall larger bone–implant distance **BID** when compared with the other two groups ($p < 0.05$, Fig. 5C). There was no significant difference in all the measured analyses between the Micromotion 1× and the Unloaded control group (Figs. 5A, B and C).

3.2. Gene expression profile

As indicated in Section 2, only samples with high RNA quality and integrity were used; the RIN values range was between 8.5 and 9.3. Analysis of the microarray results revealed different gene expression profiles during osseointegration between all the groups at day 7 post-surgery (see Table 3).

Differentially expressed genes were classified into various biological processes (BP) in order to evaluate their functional significance. The pie charts show the proportional distribution of up- (Figs. 6A, C and E) and downregulated processes (Figs. 6B, D and F) at 7 day post-surgery. A detailed list of differentially expressed genes and is presented in Supplementary Tables S1–S3.

To determine the local signaling pathways associated with tissue healing response, we further analyzed our microarray expression data using IPA software and results are listed in Supplementary Tables S4–S6. These results indicate that the predominant pathway activated in all cases were the inflammatory and immune response pathway one.

3.3. Finite element analysis

The first key result from the FE analysis was that when fibrin existed in the gap interface (Young's elastic modulus ~ 0.05 MPa), the applied force on the implant moved it axially downward about 94 μm (Fig. 7A). This motion produced a strain distribution in the fibrin (Fig. 7B) with the largest strain concentrated near the irregularities in the implant's geometry such as the crests of the threads and corners of the apex (strain concentrations); magnitudes of principal compressive strains reached as much as 60% at localized regions at the crests of the threads, and near 30% beneath the apex of the screw. This was true also for principal tensile strains (data not shown). In between the screw threads, however, principal strain magnitudes were much smaller, 10% or less.

The second key result from the FE analysis was that in models where the applied loading remained the same (as enforced in our in vivo trials), an increase in the modulus of the interfacial region (say, from 0.05 MPa for fibrin to about 0.1 or 1 MPa for organized collagenous matrix) decreased the implant's axial micromotion along with strain magnitudes in the interface (Figs. 8A–D). This proved to be significant in suggesting an explanation for differences observed in histological results for implants subjected to loading sessions for 1×/day vs. 2×/day – as discussed shortly.

4. Discussion

We have exploited a loading system that allows investigations of the relationships among mechanics, histological parameters, and the complex set of genes that relate to healing around implants placed in bone. The rationale for selecting a BIGI was to allow a closer look at the influence of loading and strains on bone induction and formation in a tissue environment that simulates the gap regions (small or large) that usually exist around any bone implant. In contrast to control (unloaded) implants and those undergoing only one loading session per day, we have shown here that simply doubling the number of loading sessions can induce major changes at the bone-implant interface. The **BFA_0** (region nearest

to the implant), the **BIC**, and the **BID** were clearly affected in the Micromotion 2× group, correlating with the presence of an intervening fibrous layer all around the implant and change in expression of genes belonging to the immune and inflammatory pathway.

Our intention was to apply a loading protocol whereby the implant is exposed to more or less the same force from day to day in an intermittent way. Previous studies by our group and others have often instead focused on maintaining a constant displacement (micromotion) of the implant relative to the surrounding healing tissue (Jariwala et al., 2017; Leucht et al., 2007; Wazen et al., 2013a, 2013b). As evidenced in plots of interfacial stiffness vs. post-implantation time illustrated in Wazen et al. (2013a)), the tissue in the BIGI stiffens (increased its modulus) over time even as the implant is displaced the same distance each day. In this instance, the applied force has to be increased over time in order to achieve the same daily displacement. These prior studies demonstrated that even with a constant interfacial displacement as large as 150 μm, healing could still occur in the majority of a gap interface, but not at high strain regions persisting within tens of microns near the implant (Leucht et al., 2007; Wazen et al., 2013b). Our results here show that healing can also occur under constant force in the majority of the interface, at least if the number of loading cycles per day is not too large.

Our results generally agree with what has been observed during bone healing in the absence of implants (Meyer et al., 1999; Rubin and McLeod, 1994). Along these lines, there are at least 4 key factors that appear to be involved: **1)** the magnitude of interfacial strain in any given cycle of loading; **2)** the number of cycles that occur in any one loading session; **3)** the number of times per day that a session of loading (and interfacial straining) occurs; and **4)** total number of cycles that accumulate during the loading sessions. We demonstrate here that doubling the number of loading sessions per day affects what transpires at the bone implant interface. So far, our work cannot determine the relative impact of the frequency of loading by itself vs. the number of cumulated cycles of loading (and related interfacial strain). Further studies comparing the same number of loading sessions but varying the number of cycles per session are required to address this question.

Concerning strain magnitude, it is already recognized in fracture fixation and interfacial bone healing that high magnitudes of strain (e.g., larger than 30%) can produce deleterious outcomes such as nonunions or formation of interfacial fibrous tissue at bone-implant interfaces (De Smet et al., 2005; Perren, 2002; Piccinini et al., 2016; Rubin and McLeod, 1994; Szmukler-Moncler et al., 1998). In our previous studies with implants in mice (Wazen et al., 2013a), we demonstrated that large strains (above about 30%) interfered with bone healing immediately next to the implants by day 7 in a constant micromotion experiment using 150 μm; in this type of experiment, each cycle of displacement creates large strains at strain-concentrating regions of the implant. Wazen et al. (2013a) also showed, however, that 2 daily sessions of 60 cycles per session of prescribed implant micromotion (150 μm) created different results in the interface than a single session of 60 cycles of the same prescribed implant micromotion. In the present work in rats, we have also found that two sessions per day of the same force (but not the same displacement) on the implant also pre-empted the progress or extent of the interfacial healing. The likely explanation behind this finding can be suggested from the results of a finite element model. First, consider

the strain magnitudes in between the crests of the threads and beneath the implant vs. the strains at the crests of the threads; locally at the crests of the threads high stains (e.g., > 50%) develop in the interface at day 1, but in between the threads and beneath the apex, the strains are much smaller (e.g., 10% or less). So even while the large strains may cause local cellular and tissue damage at the thread crests, the regions in between the threads and beneath the implants (where strains are just barely problematic at about 30% or less) can begin to form bone matrix and stiffen those regions of the interface. In turn, that local stiffening (i.e., increase in modulus) in between the threads and at the base will result in less micromotion per applied force; in turn, that stiffening will diminish the interfacial strains further, thereby favoring even more bone formation, including at the crests of the threads. A possible explanation as to why there is a markedly deleterious effect in the 2×/day protocol vs. the 1×/day protocol is that in the 2×/day protocol, the high strain regions of the interface are accumulating twice as much damage due to the two loading sessions in each day. Thus, whatever damage has accumulated during the high strain sessions has less time to recover (start to repair) before the next strain session starts. This situation repeats every day for 7 days, thus leading to an interference in bone healing at the sites of highest strains near the implant, e.g., around the threads and immediately beneath the implant. But at the same time, farther away from the bone-implant boundary, undisturbed healing can occur.

While the $\mathbf{BFA_0}$ is reduced in the animal receiving two loading sessions/day, surgical placement of an implant into the marrow and application of a controlled force to the implant are not sufficient to affect bone formation within the wider volume of marrow surrounding the surgical site. We believe this is because (1) bone marrow disruption during drilling activates a bone modeling sequence (Schulte et al., 2013; Suva et al., 1993) that is independent of the implant, and (2) the stress/strains generated by micromotion have a limited extension from the implant surface. For example, our FE analyses reveal that once the majority of the interfacial region has started to heal and increase its modulus, then at a distance of about 150 μm from the implant the strain magnitudes have fallen off to less than 0.2%, which is small and unlikely to have any significant effect on healing. So, from this standpoint, it is not surprising that, at 7 days post implantation, all groups showed similar $\mathbf{BFA_t}$ values. This was essentially confirmed by the fact that bone-related genes were detected but not differentially-expressed in our arrays (data not shown).

When the number of loading sessions per day was doubled, there was an intervening fibrous layer between the implant surface and newly-formed bone, While the DNA microarray data might appear disappointing in not pinpointing specific clues to this histological finding, they do provide compelling information showing that the force applied and resulting implant micromotion were not sufficient to alter the ongoing anabolic/catabolic pathways related to overall osteogenesis along most of the interface. While elucidating the origin of this fibrous layer will require looking at earlier intervals (e.g. 3 days), our gene profiling data is consistent with the hypothesis that it results from an immune and inflammatory response to accumulation of tissue damage in regions of high strains in the gap interface (see above FE discussion). The importance and unexpected differential expression of unidentified genes also indicates that a number of unsuspected ‘players’ are involved in implant osseointegration, and these may represent potential targets for promoting bone formation

around implants. Because the interfacial site is essentially ‘primed’ for bone formation due to the major surgical insult from the drilling and marrow disruption (Fahlgren et al., 2013; Morelli et al., 2015; Morgan et al., 2015; van der Meulen et al., 2009) it is difficult to separate what is due to background bone induction from changes induced by the application of force itself. This would be best addressed by letting the surgical site heal for a short period of time so that bone formation stabilizes before applying force. Irrespectively, loading the implant twice a day for 7 days in a row was sufficient to change interfacial healing. This could be due to (1) interfering with bone formation or (2) causing bone resorption very near the implant surface. The presence of some osteoclasts in the vicinity of the implants reflects the normal remodeling process of embryogenic new bone (Nanci, 1998; Nanci et al., 1994; Slaets et al., 2007). Our histological and molecular data, at least at the 7-day time-point, do not suggest that the level of force applied exacerbates osteoclastic activity.

Some concerns might be raised due to unequal exposure of various groups to anesthesia. The unloaded group (wound cleaning) and the Micromotion 1× group (micromotion and wound cleaning) were only anesthetized once a day, while animals in the Micromotion 2× group where anesthetized twice a day. Scattered reports mention that anesthesia can have some influence on the immune/inflammatory response (Cao et al., 2018; Cruz et al., 2017; Li et al., 2017) and consequently could have an impact on the histological and gene expression healing response. With respect to isoflurane used in our study, it has been reported that the effect of both single and repeated isoflurane anesthesia in C57BL/6JRj mice for periods of 45 min rates as mild, with only short-term distress (Hohlbaum et al., 2017) usually relating to cognitive impairment. Compared to this study, our groups only received anesthesia for maximum 5 min at a time, suggesting that isoflurane effect would be much milder. Furthermore, most anesthetics actually provide benefits with respect to local inflammation (see, as an example, Cruz et al., 2017) and isoflurane conditioning promotes the survival of stromal bone marrow cells (Sun et al., 2015). This would yield to an immune/inflammatory gene response opposite to the exacerbated one observed in our micromotion 2× group. Therefore, we suggest that our short isoflurane anesthesia had little, if any impact on the outcome of our results, and that the short supplemental isoflurane anesthesia in the 2× group did not alter significantly the outcome.

In conclusion, using a rat tibia model, application of 60 cycles of a 1.5 N maximum axial force were delivered to the head of the implant each day for 7 days, and the strains/stress induced no significant effect on the overall bone healing. As such, this level of force could be considered 'acceptable'. However, the accumulation of interfacial tissue deformation caused by doubling the number of loading sessions/day affects bone formation in the immediate vicinity of the implant and leads to the deposition of a fibrous layer along its surface, even at such ‘acceptable’ level of force. Gene expression analysis highlights the participation of the immune/inflammatory pathway and unknown genes. In this context, while not excluding the pertinence of stimulating bone formation, dealing with the sequels of excessive micromotion may be dealt with by intervening on the immune/inflammatory response chemically or biologically.

Supplementary Material

Refer to Web version on PubMed Central for supplementary material.

Acknowledgments

We extend our thanks to Prof. Dr. Florin Amzica (Universite de Montreal) for his review assistance concerning the impact of the unequal exposure of isoflurane between the groups in bone healing raised by one of the reviewers. The authors acknowledge the services from Génome Québec Innovation Center at McGill University (Montreal, Quebec, Canada) for performing the DNA microarray analysis.

Funding sources

This work was supported by National Institutes of Health, USA (NIH, 5R01DE024000-13) and Canadian Institute of Health Research (CIHR, 362821) grants. Antonio Nanci holds a Canada Research Chair in Calcified Tissues, Biomaterials, and Structural Imaging.

References

Birkhold AI Razi H Duda GN Weinkamer R Checa S Willie BM Mineralizing surface is the main target of mechanical stimulation independent of age: 3D dynamic in vivo morphometry Bone 2014 66 15–25 [PubMed: 24882735]

Brunski JB In vivo bone response to biomechanical loading at the bone-dental implant interface Adv. Dent. Res 1999 13 99–119 [PubMed: 11276755]

Cao Y, Li Z, Ma L, Ni C, Li L, Yang N, Shi C, Guo X. Isofluraneinduced postoperative cognitive dysfunction is mediated by hypoxiainducible factor1-alphadependent neuroinflammation in aged rats. Mol. Med. Rep. 2018

Cruz FF, Rocco PRM, Pelosi P. Anti-inflammatory properties of anesthetic agents. Crit. Care. 2017; 21

De Smet E Jaecques S Vandamme K Vander Sloten J Naert I Positive effect of early loading on implant stability in the bi-cortical guinea-pig model Clin. Oral Implants Res 2005 16 402–407 [PubMed: 16117763]

Duyck J Vandamme K Geris L Van Oosterwyck H De Cooman M Vandersloten J Puers R Naert I The influence of micro-motion on the tissue differentiation around immediately loaded cylindrical turned titanium implants Arch. Oral Biol 2006 51 1–9 [PubMed: 15922992]

Duyck J Slaets E Sasaguri K Vandamme K Naert I Effect of intermittent loading and surface roughness on peri-implant bone formation in a bone chamber model J. Clin. Periodontol 2007 34 998–1006 [PubMed: 17935504]

Fahlgren A Yang X Ciani C Ryan JA Kelly N Ko FC van der Meulen MC Bostrom MP The effects of PTH, loading and surgical insult on cancellous bone at the bone-implant interface in the rabbit Bone 2013 52 718–724 [PubMed: 22613252]

Geris L Vandamme K Naert I Vander Sloten J Duyck J Van Oosterwyck H Application of mechanoregulatory models to simulate peri-implant tissue formation in an in vivo bone chamber J. Biomech 2008 41 145–154 [PubMed: 17706229]

Haiat G Wang HL Brunski J Effects of biomechanical properties of the bone-implant interface on dental implant stability: from in silico approaches to the patient's mouth Annu. Rev. Biomed. Eng 2014 16 187–213 [PubMed: 24905878]

Hohlbaum K, Bert B, Dietze S, Palme R, Fink H, Thone-Reineke C. Severity classification of repeated isoflurane anesthesia in C57BL/6JRj mice-assessing the degree of distress. PLoS One. 2017; 12 :e0179588. [PubMed: 28617851]

Jariwala SH Wee H Roush EP Whitcomb TL Murter C Kozlansky G Lakhtakia A Kunselman AR Donahue HJ Armstrong AD Lewis GS Time course of peri-implant bone regeneration around loaded and unloaded implants in a rat model J. Orthop. Res 2017 35 997–1006 [PubMed: 27381807]

Leucht P Kim JB Wazen R Currey JA Nanci A Brunski JB Helms JA Effect of mechanical stimuli on skeletal regeneration around implants Bone 2007 40 919–930 [PubMed: 17175211]

Li Z Ni C Xia C Jaw J Wang Y Cao Y Xu M Guo X Calcineurin/nuclear factor-kappaB signaling mediates isoflurane-induced hippocampal neuroin-flammation and subsequent cognitive impairment in aged rats Mol. Med. Rep 2017 15 201–209 [PubMed: 27909728]

Meyer U Wiesmann HP Kruse-Losler B Handschel J Stratmann U Joos U Strain-related bone remodeling in distraction osteogenesis of the mandible Plast. Reconstr. Surg 1999 103 800–807 [PubMed: 10077068]

Morelli F Lang NP Bengazi F Baffone D Vila Morales CD Botticelli D Influence of bone marrow on osseointegration in long bones: an experimental study in sheep Clin. Oral Implants Res 2015 26 300–306 [PubMed: 25263617]

Morgan TG Bostrom MP van der Meulen MC Tissue-level remodeling simulations of cancellous bone capture effects of in vivo loading in a rabbit model J. Biomech 2015 48 875–882 [PubMed: 25579991]

Munster S Jawerth LM Fabry B Weitz DA Structure and mechanics of fibrin clots formed under mechanical perturbation J. Thromb. Haemost 2013 11 557–560 [PubMed: 23489915]

Nanci A Mccarthy GF Zalzal S Clokie CML Warshawsky H Mckee MD Tissue-response to titanium implants in the rat tibia – ultrastructural, immunocytochemical and lectin-cytochemical characterization of the bone-titanium interface Cell Mater 1994 4 1–30

Nanci AM,M Zalzal S Sakkal S Davidovitch ZM,J Ultrastructural and immunocyto-chemical analysis of the tissue response to metal implants in the rat tibia Biological Mechanisms of Tooth Eruption, Resorption and Replacement by Implants Harvard Society for the Advancement of Orthodontics 1998 487–500

Perren SM Evolution of the internal fixation of long bone fractures – the scientific basis of biological internal fixation: choosing a new balance between stability and biology J. Bone Jt. Surg. Br 2002 84b 1093–1110

Piccinini M Cugnoni J Botsis J Ammann P Wiskott A Peri-implant bone adaptations to overloading in rat tibiae: experimental investigations and numerical predictions Clin. Oral Implants Res 2016 27 1444–1453 [PubMed: 26864329]

Rubin CT, McLeod KJ. Promotion of bony ingrowth by frequency-specific, low-amplitude mechanical strain. Clin. Orthop. Relat. Res. 1994; 165 :174.

Schulte FA, Ruffoni D, Lambers FM, Christen D, Webster DJ, Kuhn G, Muller R. Local mechanical stimuli regulate bone formation and resorption in mice at the tissue level. PLoS One. 2013; 8

Slaets E Carmeliet G Naert I Duyck J Early trabecular bone healing around titanium implants: a histologic study in rabbits J. Periodontol 2007 78 510–517 [PubMed: 17335375]

Sun Y Li QF Yan J Hu R Jiang H Isoflurane preconditioning promotes the survival and migration of bone marrow stromal cells Cell. Physiol. Biochem 2015 36 1331–1345 [PubMed: 26159215]

Suva LJ Seedor JG Endo N Quartuccio HA Thompson DD Bab I Rodan GA Pattern of gene expression following rat tibial marrow ablation J. Bone Miner. Res 1993 8 379–388 [PubMed: 8456591]

Szmukler-Moncler S Salama H Reingewirtz Y Dubruille JH Timing of loading and effect of micromotion on bone-dental implant interface: review of experimental literature J. Biomed. Mater. Res 1998 43 192–203 [PubMed: 9619438]

van der Meulen MC Yang X Morgan TG Bostrom MP The effects of loading on cancellous bone in the rabbit Clin. Orthop. Relat. Res 2009 467 2000–2006 [PubMed: 19459022]

Vandamme K Naert I Geris L Sloten JV Puers R Duyck J Histodynamics of bone tissue formation around immediately loaded cylindrical implants in the rabbit Clin. Oral Implants Res 2007a 18 471–480 [PubMed: 17517061]

Vandamme K Naert I Geris L Vander Sloten J Puers R Duyck J The effect of micro-motion on the tissue response around immediately loaded roughened titanium implants in the rabbit Eur. J. Oral Sci 2007b 115 21–29 [PubMed: 17305713]

Wazen RM Currey JA Guo H Brunski JB Helms JA Nanci A Micromotion-induced strain fields influence early stages of repair at bone–implant interfaces Acta Biomater 2013a 9 6663–6674 [PubMed: 23337705]

Wazen RM Kuroda S Nishio C Sellin K Brunski JB Nanci A Gene expression profiling and histomorphometric analyses of the early bone healing response around nanotextured implants Nanomedicine 2013b 8 1385–1395 [PubMed: 23286527]

Willie BM Yang X Kelly NH Han J Nair T Wright TM van der Meulen MCH Bostrom MPG Cancellous bone osseointegration is enhanced by in vivo loading Tissue Eng. Part C-Methods 2010 16 1399–1406 [PubMed: 20367497]

Yang X Willie BM Beach JM Wright TM van der Meulen MC Bostrom MP Trabecular bone adaptation to loading in a rabbit model is not magnitude-dependent J. Orthop. Res 2013 31 930–934 [PubMed: 23423863]

Zhang X Duyck J Vandamme K Naert I Carmeliet G Ultrastructural characterization of the implant interface response to loading J. Dent. Res 2014 93 313–318 [PubMed: 24389808]

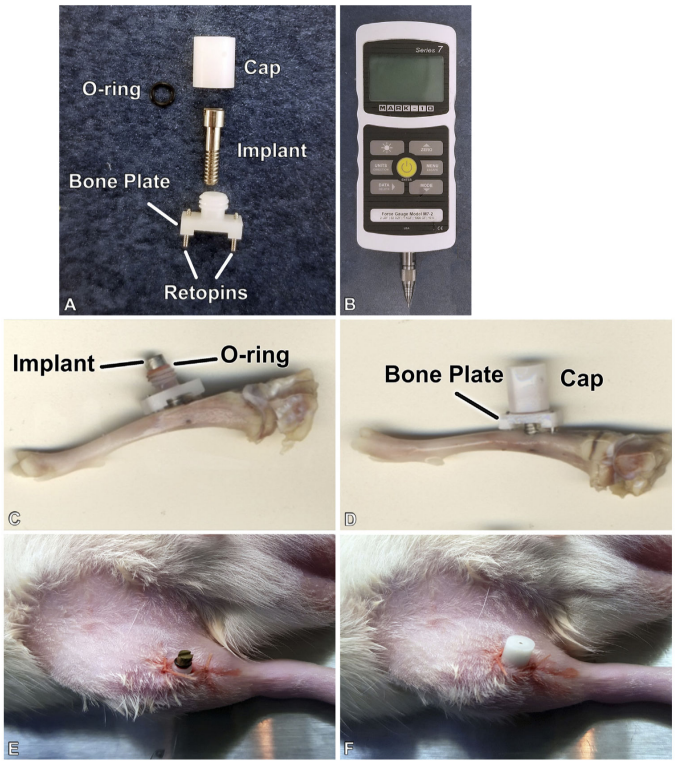

Fig. 1.

Photograph of the implant and micromotion system for rat tibiae (**A**), Mark-10 Force Gauge loading component (**B**), the implant and motion device adapted in situ in the proximal tibia metaphysis. (**C–F**) A cap protects the implant from accidental external forces (**D,F**).

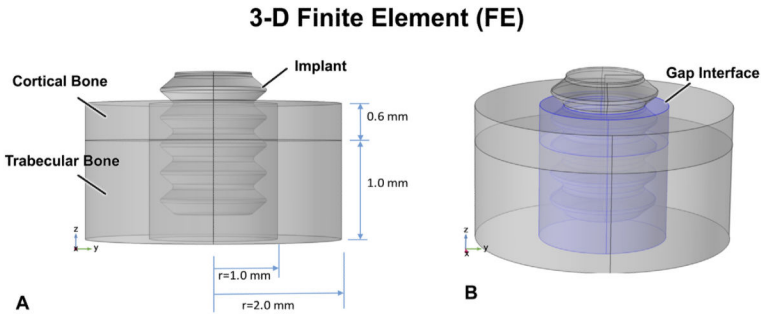

Fig. 2.

In the FE model, the bone site is idealized as being cylindrical with a 0.6 mm-thick cortical bone having trabecular bone underneath (**A**). However, the "gap" interface (**B**, blue shading in right figure) – produced by the 2 mm diameter drill – surrounds the 1.7 mm-diameter implant; the mechanical properties of this gap region can be altered to explore the influence of healing. The top surface of the implant is loaded as per the protocols described. The sides and base of the FE model are constrained.

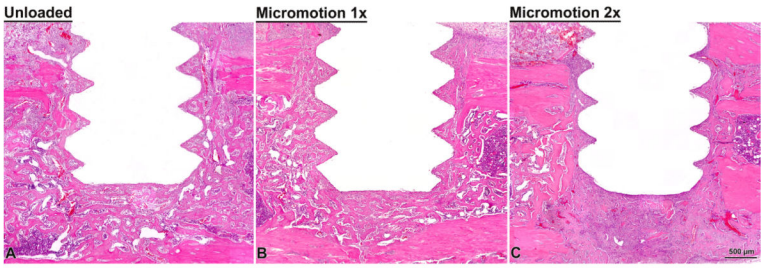

Fig. 3.

Light microscope images of decalcified sections, stained with HE, from the unloaded (**A**), micromotion 1× (**B**) and micromotion 2× (**C**) groups at 7 days post-surgery. Histological observations revealed that new bone forms around the implant in all groups, including between the implants threads. However, signs of disruption of bone healing at the bone/implant interface were noticed in all the animals from the Micromotion 2× group.

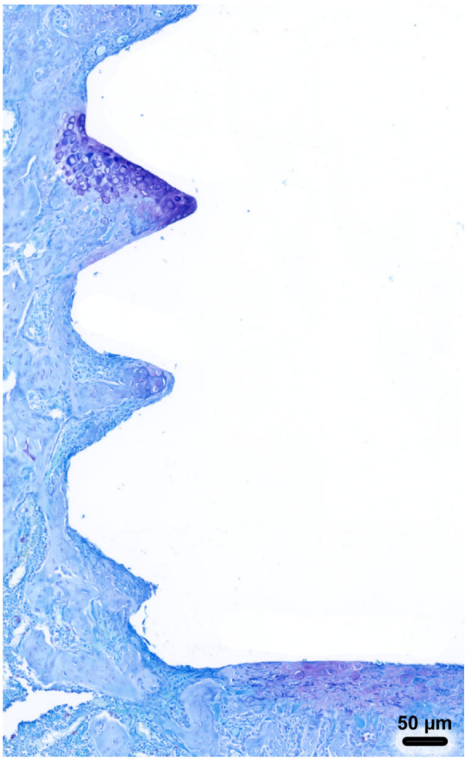

Fig. 4.
Light microscope images of decalcified sections, stained toluidine blue showing cartilage formation in a single micromotion 2× rat.

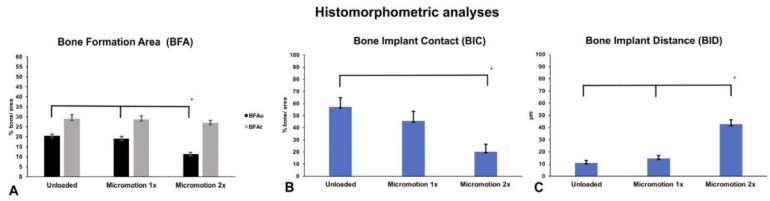

Fig. 5.

Histomorphometry of bone formation in Unloaded, Micromotion 1× and Micromotion 2× groups at 7 days post-surgery. The Micromotion 2× group showed overall lower bone formation in the interface implant/bone in the BFAo area (A), lower bone implant contact (BIC, **B**) and larger bone–implant distance (BID, **C**).

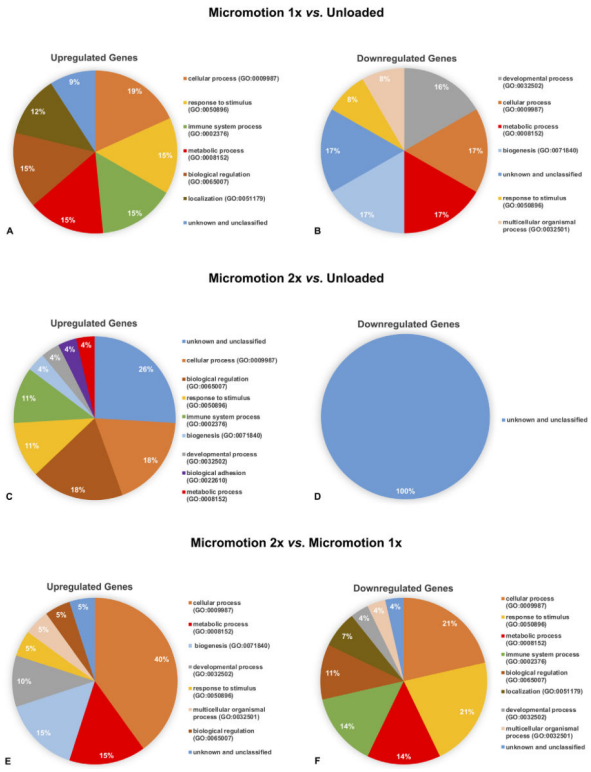

Fig. 6.

Pie charts presenting the percentage distribution of biological process ontologies identified for statistically significant genes ($p < 0.05$) differentially upregulated **(A, C, E)** and downregulated **(B, D, F)** between Micromotion 1× group vs. Unloaded group **(A, B)**, Micromotion 2× group vs. Unloaded group **(C, D)**, Micromotion 2× group vs. Micromotion 1× group **(E, F)** at day 7 post-surgery.

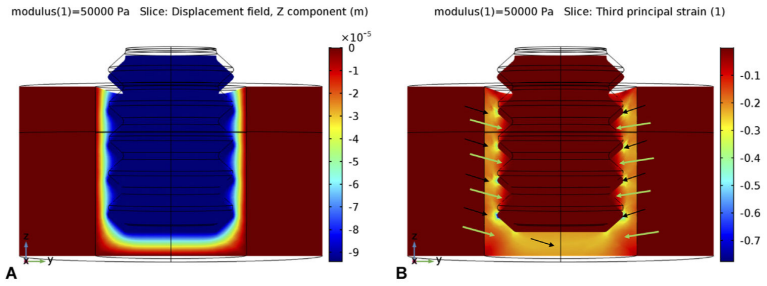

Fig. 7.

When the implant is axially loaded immediately after implantation, a fibrin clot in the gap interface has a low modulus (~ 0.05 MPa). The loading causes axially-downward micromotion (negative z-direction) of about 93 μm (**A** below). In turn, this micro-motion creates strain in the interface (**B**, below): Principal compressive strains (and tensile strains, not shown) reach high magnitudes (> 30%) near the implant's apex, and even higher values (> 60%) near the tips of the threads (black arrows). However, in between the tips of the threads and farther away from the apex (green arrows), stains are more moderate (~ 10%) and permissible for the initial stages of bone healing, e.g., collagen formation.

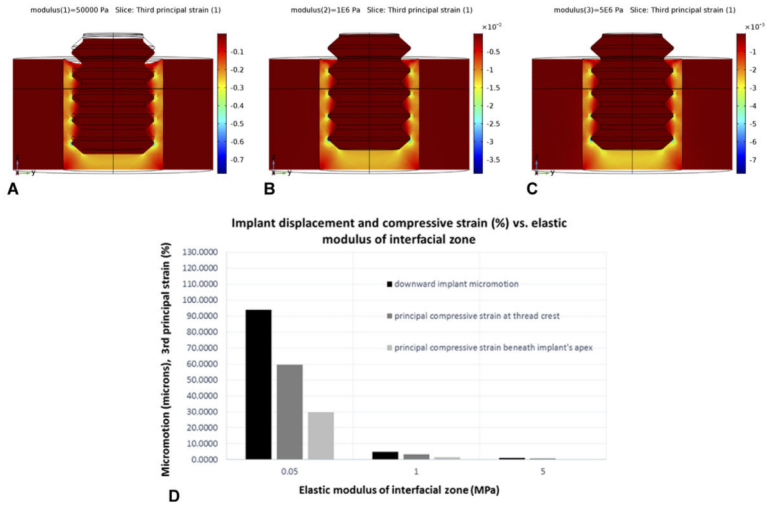

Fig. 8.

In regions in the gap where compressive strains are small to moderate, bone healing can occur, which has the effect of increasing the gap's properties (e.g., elastic modulus). In turn, that will stiffen the gap, thereby decreasing implant micromotion (under the same applied force level) as well as the strain. However, the degree of bone regeneration in the gap depends on a “race” between local damage accumulation in locations with initially high strain vs. bone regeneration in locations with low/moderate strain (as explained in the text). Note that the color bars denoting strain magnitude are different **A–C**; strains are much larger in A than in B and C because the modulus values for the gap region increase from 0.05 MPa, 1 MPa, and 5 MPa in A, B, and C respectively. For the same magnitude of axial force on the implant (**D**), the axial micromotion of the implant decreases substantially as the elastic modulus of the interfacial gap increases. Likewise, the magnitude of the peak strains in the gap decreases with increasing modulus of the interfacial gap.

Table 1

Experimental groups and loading regimen.

	Group	*Number of animals*
1	**Unloaded**	9
2	**Micromotion 1**×−60 cycles/1×-day, 7 days	9
3	Micromotion 2×−60 cycles/2×-day, 7 days	9

Table 2

Mechanical properties used in the FE model.

Region of model	Young's elastic modulus (MPa)	Poisson's ratio
cortical bone	1000	0.33
cancellous marrow	50	0.33
interfacial gap	0.05 (immediately following implantation)	0.33
implant	105.000	0.33

Table 3

Summary of microarray analysis.

Summary of microarray analysis							
GROUPS	***Total number differentially expressed genes***	***Total number upregulated genes***	**Upregulated unknown and unclassified genes**	***Number upregulated genes***	***Total number downregulated genes***	**Downregulated unknown and unclassified genes**	***Number downregulated genes***
Micromotion 1× vs. Unloaded	17	11	1	10	6	2	4
Micromotion 2× vs. Unloaded	39	19	7	12	20	20	0
Micromotion 2× vs. Micromotion 1 ×	20	10	1	9	10	1	9